LANGMUIR

pubs.acs.org/Langmuir Article

Stiffness of Fluid and Gel Phase Lipid Nanovesicles: Weighting the Contributions of Membrane Bending Modulus and Luminal Pressurization

Andrea Ridolfi,* Lucrezia Caselli, Matteo Baldoni, Costanza Montis, Francesco Mercuri, Debora Berti, Francesco Valle,* and Marco Brucale*

Cite This: *Langmuir* 2021, 37, 12027−12037 Read Online

ACCESS | Metrics & More | Article Recommendations | Supporting Information

ABSTRACT: The mechanical properties of biogenic membranous compartments are thought to be relevant in numerous biological processes; however, their quantitative measurement remains challenging for most of the already available force spectroscopy (FS)-based techniques. In particular, the debate on the mechanics of lipid nanovesicles and on the interpretation of their mechanical response to an applied force is still open. This is mostly due to the current lack of a unified model being able to describe the mechanical response of both gel and fluid phase lipid vesicles and to disentangle the contributions of membrane rigidity and luminal pressure. In this framework, we herein propose a simple model in which the interplay of membrane rigidity and luminal pressure to the overall vesicle stiffness is described as a series of springs; this approach allows estimating these two contributions for both gel and fluid phase liposomes. Atomic force microscopy-based FS, performed on both vesicles and supported lipid bilayers, is exploited for obtaining all the parameters involved in the model. Moreover, the use of coarse-grained full-scale molecular dynamics simulations allowed for better understanding of the differences in the mechanical responses of gel and fluid phase bilayers and supported the experimental findings. The results suggest that the pressure contribution is similar among all the probed vesicle types; however, it plays a dominant role in the mechanical response of lipid nanovesicles presenting a fluid phase membrane, while its contribution becomes comparable to the one of membrane rigidity in nanovesicles with a gel phase lipid membrane. The results presented herein offer a simple way to quantify two of the most important parameters in vesicle nanomechanics (membrane rigidity and internal pressurization), and as such represent a first step toward a currently unavailable, unified model for the mechanical response of gel and fluid phase lipid nanovesicles.

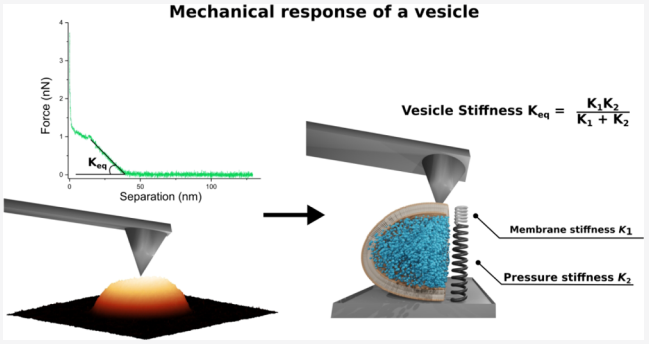

INTRODUCTION

Lipid membranes are fundamental components of most biological systems, delimiting the inner and outer compartments of cells, organelles, and viruses, hosting a significant portion of an organism's interactome and constituting a critical component of extracellular vesicles (EVs).[1] Several key biological processes were revealed to be affected by the mechanical characteristics of involved membranous compartments, including, for example, exo-/endocytosis, trafficking, and in some cases pathological onset.[2−5] Given this central role, the scientific community has devoted extended efforts for better understanding the mechanics of synthetic nanovesicles and their membranes, which represent widely used mimics for the study of biogenic membrane-bound organelles.

To this end, force spectroscopy (FS) techniques such as micropipette aspiration,[6] electrodeformation,[7] optical tweezers,[8] and atomic force microscopy (AFM)[9,10] are often employed, as they allow probing the mechanical properties at the nanoscale with high accuracy.[11] However, since it is difficult to identify and disentangle the contributions of all the parameters involved at this length scale, studying the mechanics of nanosized objects is still challenging for most of the above-mentioned techniques. In particular, the accurate determination of the nanomechanical characteristics of natural and synthetic lipid vesicles with sizes <500 nm remains a largely open issue, hindering multiple research fields.

AFM-based FS (AFM-FS) has been recently applied for studying the mechanics of both natural and synthetic lipid vesicles.[12−16] The main advantage offered by AFM-FS is the possibility to simultaneously determine the exact morphology

Received: June 22, 2021
Revised: September 13, 2021
Published: October 6, 2021

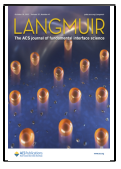

https://doi.org/10.1021/acs.langmuir.1c01660
Langmuir 2021, 37, 12027−12037

Table 1. Bending Modulus Values Reported in Literature for Fluid and Gel Phase Lipid Bilayers, Calculated Using Different Techniques

references	lipid	technique	temperature (°C)	κ ($\times 10^{19}$J)	κ (k_BT)
Liu and Nagle, 2004[53]	DOPC	scattering experiments	30	0.8	19.1
Levine, et al., 2014[54]	DOPC	atomistic simulations	25	1.1	27.7
Et-Thakafy, et al., 2017[14]	DOPC	AFM-FS on vesicles	25	0.9	21.9
Et-Thakafy, et al., 2017[14]	DOPC	AFM-FS on SLBs	25	0.9	21.4
Picas, et al., 2012[55]	DOPC	AFM-FS on SLBs	25	0.7	18.0
present study	DOPC	AFM-FS on vesicles	28	0.8	17.7
present study	DOPC	AFM-FS on SLBs	28	0.7	17.5
Dimova, 2014[56]	POPC	X-ray scattering	30	0.9	20.3
Nagle, 2017[57]	POPC	X-ray scattering	30	1.1	25.7
Henriksen, et al., 2006[58]	POPC	micropipette aspiration	25	1.6	38.5
present study	POPC	AFM-FS on vesicles	28	1.6	40.5
present study	POPC	AFM-FS on SLBs	28	2.0	49.2
Et-Thakafy, et al., 2017[14]	DPPC	AFM-FS on SLBs	25	2.0	49.3
Yi, et al., 2009[59]	DPPC	neutron spin echo	30	2.1	49.6
Picas, et al., 2012[55]	DPPC	AFM-FS on SLBs	25	2.3	56.6
Et-Thakafy, et al., 2017[14]	DPPC	AFM-FS on vesicles	25	15.5	376.7
Delorme and Fery, 2006[60]	DPPC	AFM-FS on vesicles	25	13.5	330.0
present study	DPPC	AFM-FS on vesicles	28	4.7	113.4
present study	DPPC	AFM-FS on SLBs	28	10.0	240.1
Yi, et al., 2009[59]	DSPC	neutron spin echo	40	3.4	79.1
Daillant, et al., 2005[52]	DSPC	X-ray scattering	~50	11.2	275.0
present study	DSPC	AFM-FS on vesicles	28	5.2	125.9
present study	DSPC	AFM-FS on SLBs	28	14.0	335.8

and mechanical properties of individual vesicles. In a typical AFM-FS experiment, the forces experienced by the tip during the indentation of a vesicle are recorded as a function of the tip−sample separation distance; these data are then plotted as force versus distance curves. Based on the Canham−Helfrich theory (CHT),[17,18] Vorselen et al. theorized that the initial mechanical response of a lipid vesicle to indentation is elastic and follows a linear correlation between the applied perpendicular force and the penetration depth.[19] The resulting mechanical response can be broadly described in terms of Hooke's law, $F = -Kx$, where K, the stiffness (K) of the vesicle, can be estimated from the slope of the observed linear regime. Stiffness is an extensive property resulting from multiple contributions, the most important being the intrinsic membrane elasticity and the luminal pressure (the internal pressure that originates from the fluid confined within a vesicle).

In order to quantify a vesicle's membrane intrinsic elasticity, its contribution to the experimentally accessible quantity K has to be disentangled from the others. Among the various biophysical descriptors, the bilayer bending modulus (κ) is a widely used parameter in membrane biophysics to quantify the energy required to deform a membrane from its spontaneous curvature;[20] moreover, its evaluation is of fundamental importance for understanding the effect of the membrane bending rigidity in biological processes such as vesicle fusion and budding.

Several theories and models have been proposed in the AFM-FS literature to derive κ from the measured K values, obtaining different degrees of agreement with the results from other techniques (examples can be found in Table 1). The description is further complicated by the dual nature that lipid membranes display above and below their melting temperature (T_m); at $T > T_m$, lipid bilayers are generally found in the so-called fluid phase, in which their acyl chains present an increased lateral mobility compared to the case of $T < T_m$, where membranes display the so-called gel phase, characterized by a limited lateral mobility and a tighter packing degree between the acyl chains of the two leaflets. One of the most straightforward theories used to describe the mechanics of adsorbed lipid vesicles is the thin shell theory (TST),[21] which models the lipid vesicle as being solely constituted by a homogeneous shell of thickness h and curvature radius R, provided that the ratio h/R is sufficiently small.[22] Following this approach, TST does not account for the luminal pressurization, hence ascribing all the energetic contributions of vesicle indentation to the membrane elasticity. Moreover, by describing the membrane as a single homogeneous shell, simple TST models ignore the fact that in fluid phase bilayers, the two leaflets are free to slide upon each other. Reissner[23] generalized the TST and proposed an analytical solution for the case of shallow segments of thin elastic spherical shells, which takes into consideration the presence of transverse shear deformations.[22]

More recently, both experimental and theoretical studies[19,25,26] found that the pressure contribution to the indentation response of nanosized fluid phase liposomes accounts for a great part of the overall deformation energy. Based on these findings, they developed a CHT-based model that allows calculating both the bending modulus and the luminal pressure of nanosized fluid phase lipid vesicles from their stiffness K and tether force (i.e., the force at which a lipid tube of uniform diameter is elongated away from the vesicle by the AFM tip). This model has been employed for studying the mechanical properties of EVs,[27] revealing that specific pathological conditions can induce a change in their membrane rigidity.[4]

In this context, it is immediately apparent that the two above-presented models differ irreconcilably in their treatment of the lipid bilayer, which is modeled either as a single

https://doi.org/10.1021/acs.langmuir.1c01660
Langmuir 2021, 37, 12027−12037

homogeneous shell in one case (TST) or as a pair of independently sliding monolayers in the other. These different scenarios seem at first glance most suited to describe vesicles constituted by lipids in their gel and fluid phases, respectively, thus suggesting that the applicability of the two models might be dictated by the state of the lipid membrane under investigation.

An orthogonal experimental strategy to determine via AFM-FS the κ values of membranes is to drastically simplify the problem and deposit them on a rigid substrate, obtaining supported lipid bilayers (SLBs),[28−30] whose indentation mechanics is considerably simpler to model with respect to intact vesicles. This is mainly due to the fact that the mechanical response of SLBs is not affected by internal pressure-related phenomena, hence making it possible to univocally relate the SLB indentation forces to the rigidity of the bilayer. To this purpose, various contact mechanics models have been developed to extract κ from AFM-FS experiments on SLBs.[9] Despite the extensive number of reports both on SLBs and vesicles, there is still disagreement between the κ values measured on the same membranes in the two experimental configurations. This issue further complicates the interpretation of experimental data and ultimately hinders a complete understanding of several membrane-related processes in terms of stiffness.

In an attempt to reconcile the different interpretations outlined above, we propose a simple model where the contributions of membrane rigidity and luminal pressure to the overall stiffness of a nanosized vesicle are described as a series of springs. This approach permits us to quantitatively estimate the individual contributions to the stiffness of fluid or gel phase nanosized vesicles by using a single model. We test this approach on a library of synthetic liposomes, composed of phospholipids having the same polar head group [phosphatidylcholine (PC)] but different acyl chains. This allows exploring different lipid lateral interaction energies, spanning the bilayer phase space between fluid and gel phases. All the bilayers are probed by AFM-FS both as SLBs and vesicles, allowing us to quantitatively distinguish the contributions of the membrane bending modulus and luminal pressure to the overall stiffness of the liposomes. Particle-based simulations performed on realistic models of lipid bilayers mimicking the experimental setup are then employed to support the AFM-FS results and provide new insights into the origin of the observed different mechanical responses.

EXPERIMENTAL SECTION

Vesicle Preparation. Different lipids with a PC polar headgroup [DOPC (1,2-dioleoyl-*sn*-glycero-3-phosphocholine) (>99%), POPC (1-palmitoyl-2-oleoyl-*glycero*-3-phosphocholine) (≥98.0%), DPPC (1,2-dipalmitoyl-*sn*-glycero-3-phosphocholine) (>99%), and DSPC (1,2-1,2-distearoyl-*sn*-glycero-3-phosphocholine) (>99%)] were purchased from Sigma-Aldrich (St. Louis, MO, USA). All chemicals were used as received. Lipid dry powders were dispersed in defined amounts of chloroform to prepare stock solutions. Lipid films were obtained by evaporating appropriate amounts of lipid stock solutions in chloroform under a stream of nitrogen, followed by overnight drying under vacuum. The films were swollen by a suspension in warm (50 °C) water (Milli-Q grade water was used in all preparations) to a final lipid concentration of 4 mg/mL, followed by vigorous vortex mixing. The resultant multilamellar liposomes in water were subjected to 10 freeze−thaw cycles and extruded 10 times through two stacked polycarbonate membranes with 100 nm pore size at room temperature, to obtain unilamellar liposomes with a narrow and reproducible size distribution. The filtration was performed with the Extruder [Lipex Biomembranes, Vancouver (Canada)] through Nuclepore membranes (please refer to Caselli et al.[31] for further details about the vesicle preparation and characterization).

Surface Cleaning Procedure. All reagents were purchased from Sigma-Aldrich Inc. (www.sigmaaldrich.com). Liposomes and SLBs were evaluated on microscopy borosilicate glass coverslips (Menzel Gläser) and on SiO_2 wafers, respectively. The substrates were first immersed in a 3:1 mixture of 96% H_2SO_4 and 30% v/v aqueous H_2O_2 ("oxidizing piranha") solution for 2 h in order to remove any organic residue present on their surface. Their surfaces were then cleaned in a sonicator bath (Elmasonic Elma S30H) for 30 min in acetone followed by 30 min in isopropanol and 30 min in ultrapure water (Millipore Simplicity UV). After this procedure, the substrates can be stored in ultrapure water, preserving their pristine conditions for weeks.

Surface Preparation for AFM-FS on Intact Vesicles. Cleaned glass coverslips were treated with air plasma for 15 min (air plasma cleaner, PELCO easiGlow) and incubated overnight in ultrapure water in order to maximize the silanol surface density. Slides were then functionalized by vapor-phase silanization with (3-aminopropyl)-triethoxysilane (APTES). Small batches of three to five slides were put in a desiccator with 30 μL of APTES and 10 μL of triethylamine (TEA), then a gentle static vacuum was induced by briefly engaging a rotary pump. Glass slides were then kept under these conditions for 8 h. TEA was used to promote APTES−silanol binding.[32] After that, functionalized glass coverslips can be stored in sealed Petri dishes, preserving the same surface properties for several weeks (please see the Supporting Information for surface characterization).

Surface Preparation for AFM-FS on SLBs. Cleaned silicon wafers were treated with air plasma for 15 min (air plasma cleaner, PELCO easiGlow), incubated in ultrapure water for 10 min in order to maximize the number of reactive surface silanols, and then dried with nitrogen.

SLB Formation via Vesicle Fusion. A 100 μL droplet of 200 mM $CaCl_2$ diluted 1:10 in 100 mM NaCl was spotted on a SiO_2 slide. A 10 μL droplet of the chosen vesicular dispersion was then added to the previous droplet and left incubating at room temperature for 30 min in order to promote vesicle adsorption on the surface. After that, the droplet was replaced (keeping the sample under constant hydration) by a 100 μL droplet of ultrapure water, which was then left incubating for additional 15 min. After the system equilibrated, the large droplet was gently removed, and the slide was placed in the AFM fluid cell for the measurements. This procedure is reported to promote the formation of continuous and homogeneous SLBs.[33]

AFM Setup. All AFM experiments were performed on a Bruker MultiMode 8 (equipped with NanoScope V controller electronics, a sealed fluid cell, and a type JV piezoelectric scanner) using Bruker SNL-A probes (with a triangular cantilever; nominal tip curvature radius, 2−12 nm; and nominal elastic constant, 0.35 N/m) calibrated with the thermal noise method.[34] The temperature within the fluid cell was 28 °C.

AFM Imaging. Imaging was performed in the PeakForce mode. In order to minimize vesicle deformation or rupture upon interaction with the probe, the applied force setpoint was kept in the 150−250 pN range. The lateral probe velocity was not allowed to exceed 5 μm/s. Feedback gain was set at higher values than those usually employed for optimal image quality in order to ensure minimal probe-induced vesicle deformation upon lateral contact along the fast scan axis (a comprehensive explanation of this procedure was given elsewhere[35]). The average height value of all bare substrate zones was taken as the baseline zero height reference. Image background subtraction was performed using Gwyddion 2.53.16.[36]

AFM-FS on Vesicles. In order to perform the mechanical characterization of vesicles via AFM-FS, the samples were first scanned to locate individual vesicles. The chosen vesicle was then imaged at a higher resolution (~500 × 500 nm scan, 512 × 512 points); its height profile along the slow scan axis was fitted with a circular arc taking into account values only 10 nm above the bare substrate (typical fit, $R^2 \geq 0.95$). This procedure yielded, for each

https://doi.org/10.1021/acs.langmuir.1c01660
Langmuir 2021, 37, 12027−12037

vesicle, an apparent fitted curvature radius R_C and a vesicle height value H, which were corrected as described elsewhere.[19] To avoid intrinsic piezo inaccuracy and drift, which imply a certain degree of uncertainty on both the XY position at which the force curve was constructed relative to the original image and on the maximum applied force, multiple force curves were constructed. In particular, we recorded a series of force/distance curves at multiple XY positions (typically around 64−100 curves arranged in a square array covering the vesicle initial location) for each individual vesicle. All force/distance curves were recorded at a frequency of one full approach/retraction cycle per second and a ramp size of 200−250 nm. In most cases, only a few curves showed the full mechanical fingerprint of an intact vesicle on both the approach and retraction cycles, showing a linear deformation upon applying pressure and a tether elongation plateau upon probe retraction. Of these, we first discarded those with probe-vesicle contact points occurring at probe−surface distances below the vesicle height, as measured by imaging. We then discarded traces in which the tether elongation plateau occurring during probe retraction did not extend beyond the initial contact point (further details can be found in ref 35). The remaining traces were used to calculate the vesicle stiffness (K). Multiple valid curves referring to the same vesicle resulted in very narrow distributions of K (with the average measured values taken as representative for each vesicle), while different vesicles of the same type showed much larger variations.

AFM-FS on SLBs. When performing AFM-FS on SLBs, the accuracy of the XY position at which each force curve is performed becomes less important in comparison to vesicles. We nevertheless recorded a series of force/distance curves at multiple XY positions (typically around 64−100 curves arranged in a square array covering large regions of the SLB) in order to minimize the impact of (putative) local anisotropies of either the substrate or the bilayer on the measured mechanical properties. All force/distance curves were recorded at a frequency of one full approach/retraction cycle per second and a ramp size of 200−250 nm. The recorded curves were then analyzed to extract the bending modulus (κ) values.

Particle-Based Molecular Dynamics Simulations. Particle-based molecular dynamics (MD) simulations were performed on realistic models of SLBs using the Martini coarse-grained potential.[37−39] Simulations were performed with the LAMMPS program package[40] and run on the CNR-ISMN high-performance computing facility.

The model system was composed of a 2D periodic support surface, a finite-size model of SLBs in water solution, and a model of a mechanical probe. Models of DPPC and DOPC lipid bilayers in water solution were considered. Upon equilibration onto the substrate in water, lipid bilayer models relax into a round-like shape, with a diameter of about 24 nm. A model of a mechanical probe mimicking the AFM tip was built as a disc of SG4 beads, similar to the support surface. A radius of the AFM tip model of 9 nm was considered. The mechanical properties of SLB were simulated by reproducing the displacement of the AFM tip toward the surface, which was kept fixed in simulations. A first trajectory was obtained by displacing the AFM tip toward the SLB at a constant velocity of 0.1 nm/ns. This first fast trajectory allowed us to obtain starting configurations for subsequent accurate sampling of force versus distance curves. Further details are provided in the Supporting Information section.

RESULTS AND DISCUSSION

We employed AFM-FS to measure the mechanical response of a series of lipid bilayers in their planar (SLB) and vesicular configurations. All the FS experiments were performed under the same experimental conditions (deposition protocol, solution, temperature, and substrate; see the Experimental Section). All the probed lipids have the same polar head group (PC) but differ in the length and degree of unsaturation of their hydrocarbon chains. As a general rule, short and unsaturated hydrocarbon tails generate softer lipid bilayers, while long fully saturated tails have a higher packing degree, which increases the overall bilayer rigidity. It is known from the literature that the bending modulus of lipid bilayers used in this study increases in the following order: DOPC < POPC < DPPC < DSPC[31,41,42] (with DOPC and POPC being in their fluid phase and DPPC and DSPC in their gel phase under the experimental conditions employed herein). All the four lipids were used to form liposomes and SLBs and then measured via AFM-FS.

Measurement of Vesicle Stiffness. We first measured the stiffness of several different vesicles composed of each of the lipids in the above-mentioned set (details can be found in previous works[31,35]). Despite stiffness being an extensive property, the very similar average size and narrow polydispersity of the measured liposomes resulted in a relatively small variance within each sample (as it can be seen from the small overlap between the error bars in Figure 1 and from their numerical values in the second column of Table 3). The liposomes follow the expected stiffness ranking, with DOPC liposomes being the softest and DSPC liposomes the stiffest, and the stiffness values are in close agreement with those reported in the literature for similar-sized vesicles.[19,43]

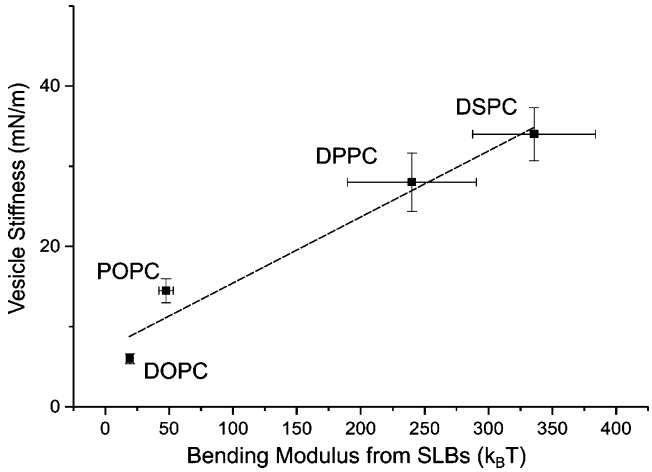

Figure 1. Linear correlation between the average vesicle stiffness K and the average SLB bending modulus κ_{SLB}. Error bars for vesicle stiffness describe the standard deviation of the mean, while the ones for κ_{SLB} of SLBs represent the uncertainties obtained by bootstrapping (1000 repetitions of 5 draws, with replacement).

Measurement of SLB Bending Modulus. We then performed AFM-FS measurements on SLBs obtained from the rupture of the same set of liposomes. The mechanical response of SLBs to indentation is much simpler to model with respect to that of vesicles; indeed, their bidimensional geometry and the absence of internal pressure contributions allow one to unambiguously probe the membrane rigidity in itself. Once the bilayer adsorbs on the substrate, it can be effectively modeled as a layer of a continuous material and hence the AFM tip can be used to apply a perpendicular force to the SLB, resulting in its compression. Fitting an appropriate contact mechanics model to the recorded indentation traces allows extracting quantitative nanomechanical information about the SLB. Among the numerous contact mechanics models developed to describe the indentation of a flat material by probes of various shapes and sizes,[9] we found that the modified Hertz model[44] proposed by Dimitriadis et al.[45] is the one that best

https://doi.org/10.1021/acs.langmuir.1c01660
Langmuir 2021, 37, 12027−12037

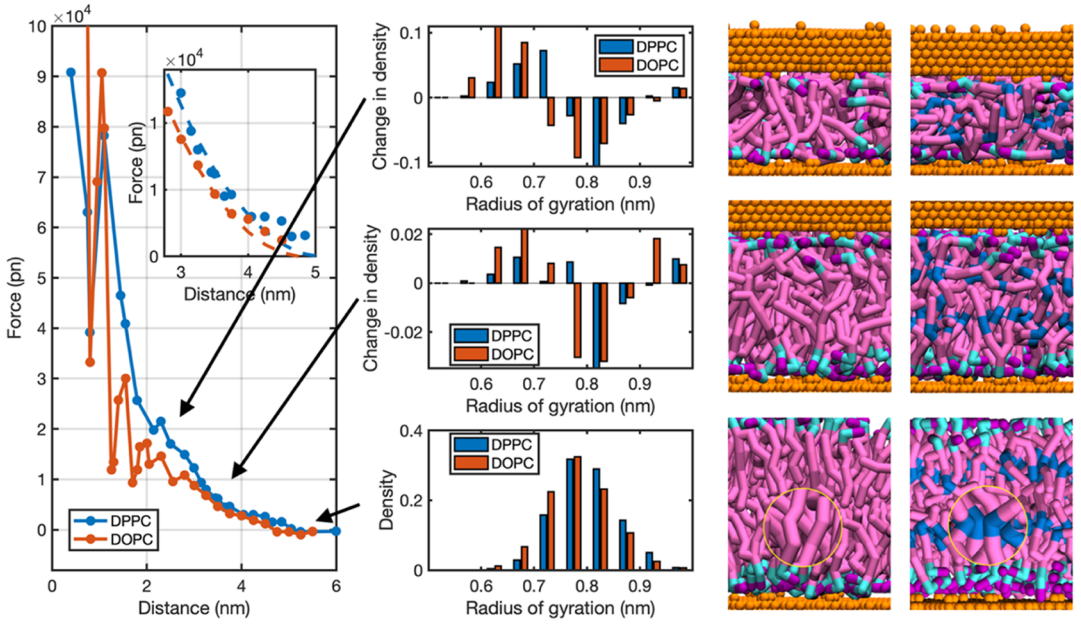

Figure 2. Simulated force/distance curves for DOPC (orange curve) and DPPC (blue curve) SLBs; dashed lines, in the inset, are the modified Hertz fits, also used for fitting the AFM-FS curves on SLBs. Distribution of the radius of gyration for configurations extracted from the points indicated by the arrow and the corresponding snapshots extracted from MD simulations. The blue segments indicate the coarse-grained beads (Martini C3 particle), describing the double-bond moiety in the structure of DOPC.

fits all our SLB indentation profiles (Figure S1). According to this model, the Young modulus of the probed bilayer can be calculated from eq 1

$$F = \frac{16}{9} E R_{tip}^{1/2} \delta^{3/2} [1 + 0.884\chi + 0.781\chi^2 + 0.386\chi^3 + 0.0048\chi^4] \quad (1)$$

where the force F is related to the Young modulus E, tip radius R_{tip}, and indentation depths δ and χ, which is equal to $\sqrt{R\delta/h}$, with h being the thickness of the bilayer (evaluated by AFM imaging experiments on different SLBs and in good agreement with the literature,[14,46−51] please refer to Figure S3 for further details). According to Saavedra et al.,[64] probing SLBs with tips having radii of ∼2 nm leads to the penetration of the lipid membrane with minimal compression and an absence of any clear mechanical event associated to membrane rupture in the force/distance traces; under these conditions, the estimation of E is not possible. However, all of our SLB indentation curves contained a clear compression region before a sharp force drop corresponding to the mechanical failure of the bilayer, suggesting that R_{tip} was always above 2 nm in our experiments. To estimate the value of R_{tip}, a subset of SLB indentation curves for each lipid was fitted, leaving the tip radius as a free parameter; this always yielded R_{tip} values in the 7−8 nm range, which would therefore allow for a correct estimation of E. TST provides a relation between the Young modulus E and the bending modulus κ; such an expression can be used to obtain the SLB bending modulus κ_{SLB} and is described in eq 2, where ν is the Poisson modulus (assumed to be 0.5[12,14] for all the following calculations).

$$\kappa = \frac{Eh^3}{12(1-\nu)} \quad (2)$$

The values obtained for the bending moduli of the whole SLB series are (17.5 ± 2.8) k_BT for DOPC, (49.2 ± 5.2) k_BT for POPC, (240.1 ± 50.4) k_BT for DPPC, and (335.8 ± 48.1) k_BT for DSPC; remarkably, they follow the same trend observed for the stiffness of the respective liposomes and are in good agreement with the vast majority of literature results, in that fluid phase bilayers typically show bending moduli around 1 order of magnitude lower than those of gel phase bilayers.[52] Table 1 reports a comparison of our results with several bending modulus values reported in the literature both for fluid and gel phase bilayers.

Vesicle Stiffness and SLB Bending Modulus Are Linearly Correlated. While the κ_{SLB} values obtained as described above are intensive (i.e., size-independent) mechanical properties, specific for each bilayer type, and the stiffness values K, measured on their vesicular configuration, are extensive properties and might be influenced by the size and/or geometry artifacts. Nevertheless, it is possible to obtain a strong indication of K being representative of the vesicles' mechanical response by plotting it against κ_{SLB} for the whole series of lipids (see Figure 1). The resulting linear correlation between mechanical descriptors, obtained from two series of independent measurements, performed with the same setup, on the same lipid bilayers, in either planar or vesicular geometry, can be considered as indicative of two facts: first, the average stiffness K is indeed a good descriptor of mechanical differences occurring across the panel of lipids, as hypothesized previously (see the section, "Measurement of Vesicle Stiffness"). Second,—despite K being a complex parameter emerging from the interplay of several concurring phenomena including vesicle geometry, bilayer bending modulus, and its resistance to pressurization—all of its determinants appear to be effectively recapitulated in just one parameter, κ.

This observation can be rationalized as follows: K values were measured on vesicles having similar sizes, same polar head group, and in the absence of an osmotic imbalance; under these conditions, any systematic difference between the mechanical responses exhibited by vesicles of different

https://doi.org/10.1021/acs.langmuir.1c01660
Langmuir 2021, 37, 12027−12037

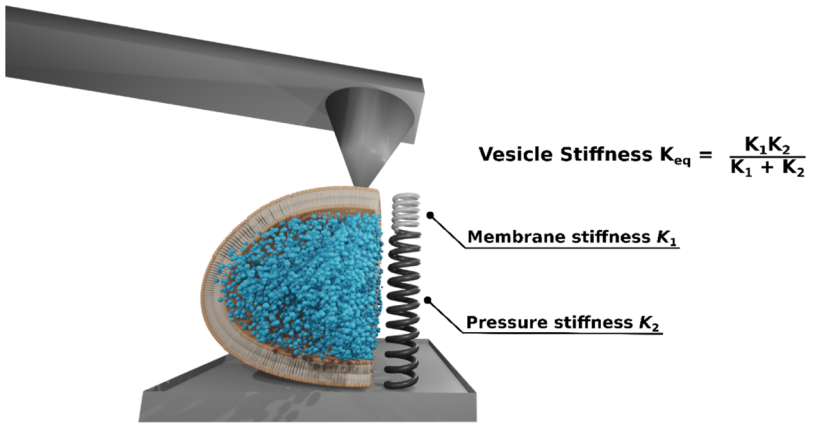

Figure 3. Spring-based model developed to describe the mechanical response of a vesicle to indentation. The stiffness of a vesicle accounts for the contributions of both membrane rigidity (mostly κ) and internal pressurization and can be described by a system of two springs in series. As a consequence, AFM-FS indentation experiments sample the overall spring constant of the whole system, which is lower than both the single spring constants K_1 and K_2.

compositions will necessarily arise from the different degrees of interaction exhibited by their constituent lipids. Different interlipidic interaction energies will ultimately determine both κ and the various phenomena contributing to K, thus resulting in the observed direct proportionality between κ_{SLB} and K. Moreover, the linear relation displayed in Figure 1 is in good agreement with Dai et al.,[61] who theorized a linear relation between the stiffness and the bending modulus of lipid nanovesicles.

MD Simulations. Coarse-grained simulations were performed on model systems of SLBs, with the aim of reproducing their response to the indentation by the AFM tip. A representative snapshot of a configuration extracted from MD simulations for the evaluation of the mechanical properties of SLBs is shown in Figure S2 (refer also to Figure S4 for further details). The two considered lipids, DOPC and DPPC, are representative of the fluid and gel states of SLBs, respectively.

The simulated force/distance curves are qualitatively very similar to the ones obtained from the AFM-FS measurements on SLBs. Moreover, the modified Hertz fit applied to the experimental force/distance curves can still be used for describing the simulated ones with remarkable accuracy (see Figure 2). The offset in the absolute value of computed forces with respect to the experiments is related to the details of the simulations (the size and shape of the simulated mechanical probe, etc.). Namely, the flat shape of the probe used in MD simulations (see Figure S2 in the Supporting Information) partially accounts for the larger overall computed force with respect to values measured for DPPC and DOPC SLBs in AFM-FS experiments.[54,62−64] This effect can be related to the higher contact area of the probe used in simulations with respect to a curved tip shape. However, the shape of the probe used to simulate force spectra allowed us to sample the dynamics of a large portion of the SLB.

In agreement with the experimental results, the DPPC SLB displays a stiffer mechanical response with respect to the DOPC SLB. At small indentations (tip−surface distances between 6 and 3 nm), the SLBs undergo an essentially elastic deformation which only entails minimal perturbations to the equilibrium configuration for both DOPC and DPPC (see Figure 2); differences in the response of the two simulated SLBs can be mainly ascribed to the different cohesive energies (hydrophobic interactions) of the bilayers. At larger indentations (tip−surface distances of ∼2.5 nm), a qualitative difference emerges for the two considered lipid species. The stiffness of the DPPC SLB still exceeds the one of the DOPC SLB, as expected; however, starting from a tip−surface distance of about 2.5 nm, the DOPC SLB undergoes a more evident structural rearrangement with respect to DPPC (see Figure 2, rightmost panels). This behavior can be related to the presence of saturated chains in the fatty acid moieties of DPPC, in contrast with the unsaturated chains of DOPC. These structural features are reproduced by the potential parameters used in simulations and lead to the observed differences in the mechanical properties of the two considered species. The occurrence of C−C double bonds in the unsaturated fatty acid chains of DOPC provides these molecules with a higher propensity to deform under a mechanical stress, with respect to those of DPPC (see Figure 2). The magnitude of this local distortion can also be visualized when computing the average radius of gyration for the individual lipid molecules constituting the bilayer. In this context, the radius of gyration provides a measure of the linearity of the molecular structure. As shown in Figure 2, the radius of gyration of DOPC molecules exhibits a significant drop in tip−surface distances below 2.5 nm, signaling molecular deformations toward a coil-like structure. These deformations affect the structure of the whole bilayer and the resulting mechanical response, as evidenced by the kinks in the computed force−displacement curves for DOPC in the range between 1 and 2 nm. Based on these results, differences in the mechanical behavior of the two considered SLBs, representative of gel and fluid phase bilayers, can be related to the interplay between intermolecular cohesion energy and intramolecular deformation. It is also worth noting that, at very large stress values, irreversible (plastic) structural deformations, falling beyond the range of elastic deformations considered by the employed model, occur. On a qualitative level, results from these simulations confirm that the different cohesion energies of fluid and gel phase lipids and the molecular structure can explain their different mechanical behaviour, as observed by AFM-FS.

A Mechanical Model for Both Fluid and Gel Phase Vesicles. The two most widely employed models for vesicles' mechanics are limited to the study of either fluid or gel phase bilayers. However, in the previous paragraphs, we have shown

https://doi.org/10.1021/acs.langmuir.1c01660
Langmuir 2021, 37, 12027−12037

that the experimentally determined vesicle stiffness K is directly proportional to the SLB bending modulus κ_{SLB}, irrespective of the phase state of the constituent bilayers, thus suggesting that their mechanical behavior can be interpreted within a unified theoretical framework.

In order to gain more insights into the relationship between the mechanical responses of a lipid bilayer in its vesicular and SLB forms, we developed a simple model that allows separating the contributions of membrane elasticity and luminal pressure from the mechanical response of a fluid or gel phase lipid vesicle subjected to an applied perpendicular force. As schematized in Figure 3, we model an adsorbed lipid vesicle as a system of two springs in series, with spring constants K_1 and K_2. The spring constant K_1 accounts for the mechanical response of the membrane, while K_2 accounts for those phenomena arising as a consequence of the volume/surface variations induced by the indentation process (the most relevant being internal pressurization).

More specifically, the slope observed in the linear part of the AFM force/distance curves (Figure S5) represents the equivalent spring constant of the system, K_{eq}, which is related to K_1 and K_2 by eq 3.

$$K_{eq} = \frac{K_1 K_2}{K_1 + K_2} \tag{3}$$

The relation expressed by eq 3 implies that the value of K_{eq} is lower than the values of both K_1 and K_2.

TST Underestimates the Mechanical Response of Gel Phase Lipid Vesicles. As detailed above, TST models a vesicle as a hollow homogeneous shell with no internal pressure.[65] Reissner[24] derived a TST-based analytical solution (eq 4) for describing the relation between force and shell indentation[66]

$$F = \left(\frac{4Eh^2}{R^2\sqrt{3(1-\nu^2)}} \right)\delta \tag{4}$$

where E is the Young modulus, h the bilayer thickness, δ the penetration depth, R the shell (vesicle) radius of curvature, and ν the Poisson modulus. Equation 4 is analogous to Hooke's law, where the term within the parentheses represents, for small penetration depths, the stiffness of the vesicle. Once K is known, E and κ can be determined, applying eqs 4 and 2. Equation 4 is designed for hollow shells; hence it assumes that the stiffness (the proportionality constant between F and δ) is only ascribed to the vesicle membrane.

According to the just-defined spring-based model, if we use the stiffness obtained from the AFM measurements, K_{eq} (a combination of K_1 and K_2) to estimate the Young modulus from eq 4, we could obtain unexpected results. Notably, since K_{eq} is lower than K_1, the mechanical contribution of the membrane and hence the values of E and κ_V (the bending modulus calculated with the vesicular configuration) are necessarily underestimated. Table 2 shows the bending moduli obtained by substituting K_{eq} into the Reissner equation for the panel of investigated liposomes and compares them with the values of the bending modulus obtained for the SLBs; the errors represent the uncertainties obtained by bootstrapping (1000 repetitions of 5 draws, with replacement).

As hypothesized, the κ_V values obtained via TST from vesicle indentation are lower than the ones obtained via the modified Hertz model from the corresponding SLBs (κ_{SLB}).

Table 2. Comparison between the Bending Modulus Values Obtained for Vesicles and SLBs

	κ_V from TST (k_BT)	κ_{SLB} from modified Hertz model (k_BT)
DOPC	17.7 ± 1.7	17.5 ± 2.8
POPC	40.5 ± 5.5	49.2 ± 5.6
DPPC	113.4 ± 20.2	240.1 ± 50.5
DSPC	125.9 ± 15.4	335.8 ± 48.1

Interestingly, the higher the vesicle stiffness, the higher the difference between κ_V and κ_{SLB}. These results support the predictions of this spring-based model; indeed, when probing very soft liposomes, such as DOPC, $K_{eq} \sim K_1$, and the Reissner formula yields results that are in good accord with the values measured on SLBs. However, as the K_1 of the probed liposomes increases and becomes proportional to K_2, the approximation is not valid anymore; K_{eq} will be lower than the other two spring constants, yielding values of κ_V lower than the respective κ_{SLB}.

Estimating the Membrane-Associated Spring Constant. Since the SLB indentation can be modeled as a 2D process, the complexity related to the 3D geometry of vesicles can be circumvented, and the contributions from the vesicle internal pressure neglected. Moreover, since the literature on SLB mechanics is well established, and there are very few uncertainties regarding data interpretation, we herein assume that the κ_{SLB} values are the ones that most closely represent the intrinsic bending rigidity of the membranes. Leveraging this assumption, if we now replace the κ_{SLB} values back in eq 2, we obtain the respective Young moduli E that can be then substituted in eq 4, in order to extract the correct values for the spring constant associated with the vesicle membrane (corresponding to the expression within parentheses in eq 4), K_1. Table 3 displays the K_1 values that we obtained for the probed vesicles and compares them with the respective K_{eq} values, calculated directly from the AFM force/distance curves.

Table 3. Spring Constant Values that Describe the Mechanical Response of a Lipid Vesicle to Indentation

	K_1 derived from SLB assumption (mN/m)	K_{eq} from the AFM curves (mN/m)	K_2 obtained by substituting K_1 and K_{eq} in (3) (mN/m)
DOPC	6.9 ± 0.3	6.0 ± 0.6	~47.3
POPC	22.7 ± 2.9	14.5 ± 1.5	~40.0
DPPC	74.4 ± 7.2	28.0 ± 3.6	~44.9
DSPC	97.4 ± 8.4	34.0 ± 3.3	~52.2

The results in Table 3 strongly support the predictions derived from the spring-based model; indeed, for very soft fluid phase vesicles (such as DOPC), we can assume that $K_1 \ll K_2$, hence obtaining $K_{eq} \sim K_1$, which means that the stiffness measured from the AFM force/distance curves (K_{eq}) is close to the actual value of the membrane stiffness (K_1). When dealing with stiffer membranes, as in the case of gel phase bilayers (DPPC and DSPC), K_1 increases and becomes comparable with K_2; in this new configuration, both the springs of the model deform (although to different extents) under application of a force. In this second scenario, the stiffness calculated from the AFM force/distance curves (K_{eq}) results from the combination of both springs (hence from the contributions of both the membrane and luminal pressure). Using the newly obtained values of K_1, we can exploit eq 3 to derive the values of K_2 for each different liposome. These

https://doi.org/10.1021/acs.langmuir.1c01660
Langmuir 2021, 37, 12027−12037

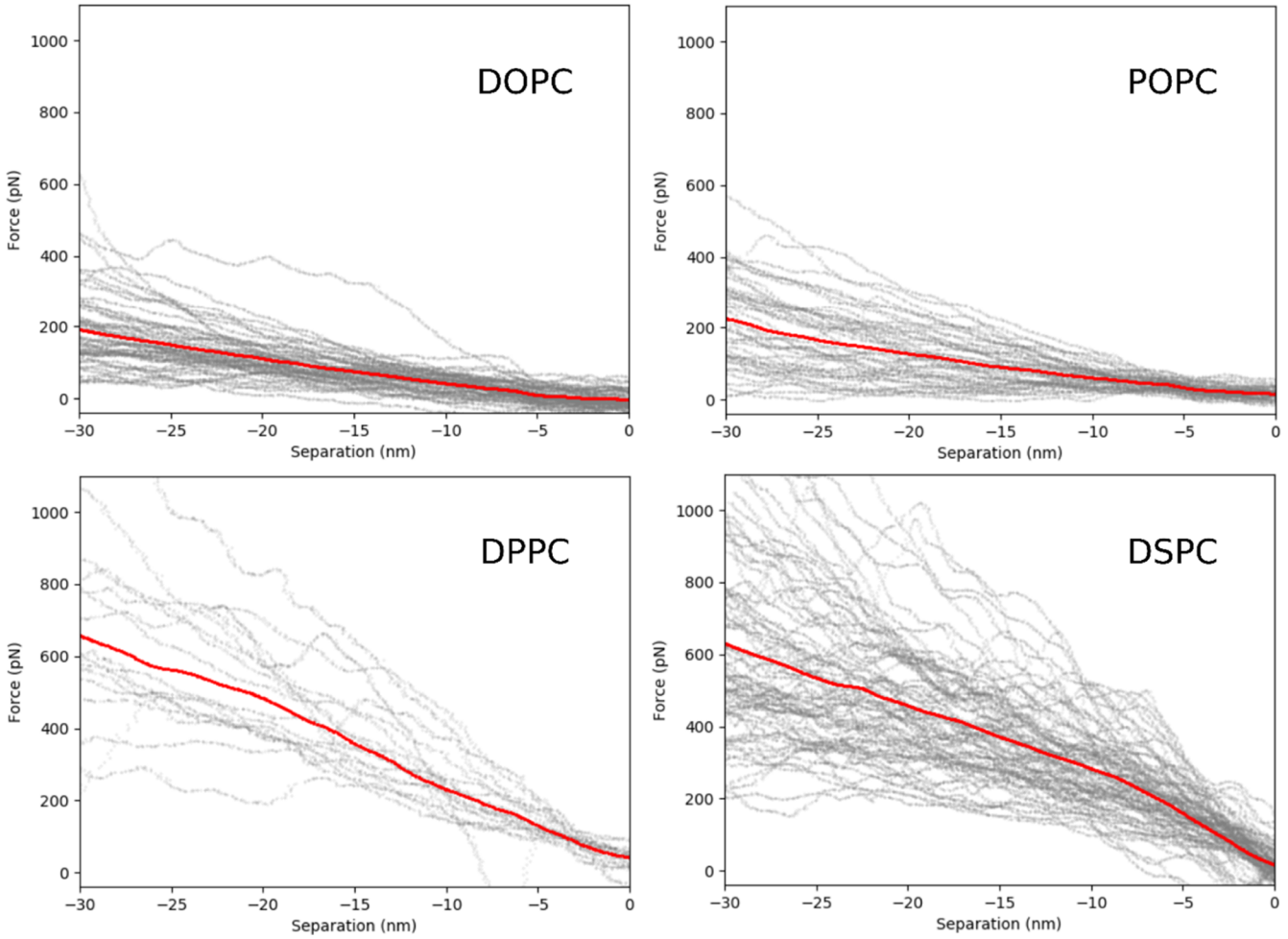

Figure 4. Average curves for the four different liposome types. Each average curve (red curve) was calculated by computing the average value of the single force/distance curves at each separation value. As can be seen, when going from DOPC to DSPC, K_1 and K_2 become comparable, and variations in K_2 due to leakages of internal fluid during the indentation may have a stronger impact on K_{eq} and on the observed curve slope.

values are shown in the third column of Table 3 and should recapitulate the mechanical contribution arising from changes in the volume/surface of the vesicles, the most relevant being the internal pressurization. Surprisingly, the estimated K_2 values are very similar for most of the probed liposomes, irrespective of their membrane phase state. Only DSPC vesicles display a slightly increased pressurization, compared to the other ones. These results suggest that the mechanical contributions from the internal pressurization of most of the probed vesicles are very similar across different liposome types. Looking at the K_2 values for the fluid phase liposomes (DOPC and POPC), it can be seen that the pressure plays a predominant role in the general mechanical response of these vesicles (with DOPC having a K_2 that is 1 order of magnitude higher than K_1), which is in perfect accord with the findings of Vorselen et al.,[19] according to which the internal pressure of fluid phase liposomes provides the most relevant contribution to the vesicles' mechanical response. The obtained results also highlight the different contributions of membrane elasticity and internal pressure to the overall vesicle stiffness, in fluid and gel phase liposomes; in the first ones, the greater contribution to the vesicle stiffness is from the internal pressure, while in the second ones, the contributions of membrane and pressure become comparable, and the vesicle mechanical response is given by their combination.

The Difference between K_1 and K_2 Could Explain the Slope Change Often Observed at Large Indentation Lengths in the AFM Force/Distance Curves. When the penetration depth is further increased (to values much larger than the membrane thickness), different events may take place: the AFM tip can puncture the bilayer (as often suggested by a sudden drop in the force signal in several vesicle indentation curves), the vesicles may lose part of their luminal content (depressurization) or even burst under excessive pressure. The manifestation of these events varies across different vesicle types; from the analysis of the force curves obtained during the AFM-FS measurements on vesicles, we found that the ratio between K_1 and K_2 could provide an interpretation of the variability in the mechanical response characterizing the second part of the force/distance curves. Figure 4 displays the force curves collected during a representative ensemble of indentation cycles performed on four different vesicle types (gray curves). Different from the calculation of the vesicle stiffness, this time, the curves were processed exploiting a custom Python script that allowed for the automatic determination of the contact point, for the subsequent alignment and for the estimation of the average curves (red traces). Due to this, occasional misalignment issues might occur, which, however, do not significantly affect the following qualitative interpretation of the results. The average curves are

https://doi.org/10.1021/acs.langmuir.1c01660
Langmuir 2021, 37, 12027−12037

obtained by averaging the values of the displayed gray curves at each separation point. As seen in Figure 4, the straightness of the red curves decreases from DOPC to DSPC, with the latter displaying a pronounced slope change.

These different behaviors can be rationalized by analyzing how K_{eq} changes when the value of K_2 is decreased. For those cases in which the overall stiffness is dominated by K_2, $K_{eq} \sim K_1$ and hence a variation in K_2 has a negligible effect on the observed curve slope (K_{eq}), as the new value of K_2 still largely exceeds K_1 (see eq 3). On the other hand, when K_2 is comparable with K_1, its variation has a stronger impact on K_{eq}, generating an appreciable change in the slope of the curve.

A decrease in K_2 could come as a consequence of larger indentations, which imply an increase in the internal pressurization of the vesicles, an event that could trigger the release of part of the internal fluid with a subsequent loss of volume. As a result, the vesicle would consequently have less fluid inside its lumen, hence being less pressurized, that is, its K_2 would have a lower value. On the other hand, since K_1 represents the membrane stiffness, which should not be affected by depressurization phenomena, its value is assumed to remain constant during the whole indentation process. According to these predictions, in Figure 4, the effect of depressurization on the curves' slope is negligible for DOPC (the curves retain the initial slope also for larger indentations), but it becomes gradually more important approaching the stiffer gel phase liposomes, where the curves display larger variability for higher indentation values. The onset of a second linear regime in the force/distance curves has also been recorded in the AFM studies of Vorselen et al.[19] and Calò et al.,[12] while Vella et al.[67] obtained a similar response from indentation tests on inflated spherical shells; most of these studies point to the pressure as the main responsible factor for the observed effect. This aspect might also explain why in stiffer liposomes, variations in the measured values of both stiffness and bending modulus are higher than those found for softer ones.

CONCLUSIONS

Lipid membranes are involved in a plethora of relevant biological processes; for this reason, characterizing their mechanical properties can help understand the fundamental interactions between interfaces at the nanoscale. FS techniques can be used to probe the mechanical properties of nanosized membranous envelopes such as vesicles, viruses, and other organelles; despite the high accuracy of these techniques, the data interpretation still stirs a debate, ultimately leading to a disagreement of the results obtained with different techniques.

By performing AFM-FS on a set of fluid and gel phase SLBs, we characterized their mechanical response in terms of bending modulus, which is an intrinsic descriptor of the membrane rigidity. Coarse-grained MD simulations performed on realistic SLBs models confirmed and supported the AFM-FS results, showing that the differences, experimentally observed between fluid and gel phase bilayers, can be ascribed to the interplay between intermolecular cohesion energy and intramolecular deformation.

Leveraging these results, we probed (by means of AFM-FS) the same set of fluid and gel phase lipid bilayers, in the liposome configuration, and found that the mechanical response of a lipid vesicle to an applied deformation can be modeled by a system of two springs in series. One of the springs accounts for the effect of membrane elasticity while the other for the effects arising from large volume/surface variations, whose greater contribution comes from the luminal pressure.

Exploiting this spring-based model, we find that despite not accounting for internal pressure contributions, the TST can still be used to extract the bending modulus values of very soft vesicles (such as DOPC), for which the spring constant representing membrane stiffness has a negligible value compared to the one representing the luminal pressure. When these two contributions become comparable, the mechanical response of vesicles is a combination of the two springs and cannot be correctly analyzed by means of TST only. By assuming that the correct values of the bending modulus are the ones obtained from the AFM-FS on SLBs, we find that the pressurization of most of the probed vesicles (which had a similar size) is similar, independent of the lipids forming the bilayer. Moreover, our mechanical model provides an interesting interpretation of the change in the slope displayed in the force curves of stiffer liposomes, showing that when the two spring constants are comparable, a change in the internal pressure would have a more appreciable effect on the vesicle stiffness, as probed through AFM-FS.

Our findings shed light on the nanomechanics of lipid vesicles and provide a possible explanation to the discrepancy that is often observed among the results of the bending modulus obtained from intact vesicles and SLBs. Future works will be aimed at quantifying the extent of the internal pressure contribution, in order to correct and hence extend the applicability of TST-based models to the description of both gel and fluid phase vesicles. Ultimately, when applied to natural vesicles, such as EVs, the simple but clear-cut insights afforded by our model might help to better understand the fundamental biological processes that involve vesicular deformation and/or reorganization.

ASSOCIATED CONTENT

Supporting Information

The Supporting Information is available free of charge at https://pubs.acs.org/doi/10.1021/acs.langmuir.1c01660.

AFM-FS measurements performed on both vesicles and SLBs and details about the MD simulations (PDF)

AUTHOR INFORMATION

Corresponding Authors

Andrea Ridolfi − *Consorzio Interuniversitario per lo Sviluppo dei Sistemi a Grande Interfase, 50019 Firenze, Italy; Istituto per lo Studio dei Materiali Nanostrutturati, Consiglio Nazionale delle Ricerche, 40129 Bologna, Italy; Dipartimento di Chimica "Ugo Schiff", Università degli Studi di Firenze, 50019 Firenze, Italy;* orcid.org/0000-0003-4224-9333; Email: andrea.ridolfi@unifi.it

Francesco Valle − *Consorzio Interuniversitario per lo Sviluppo dei Sistemi a Grande Interfase, 50019 Firenze, Italy; Istituto per lo Studio dei Materiali Nanostrutturati, Consiglio Nazionale delle Ricerche, 40129 Bologna, Italy;* Email: francesco.valle@cnr.it

Marco Brucale − *Consorzio Interuniversitario per lo Sviluppo dei Sistemi a Grande Interfase, 50019 Firenze, Italy; Istituto per lo Studio dei Materiali Nanostrutturati, Consiglio Nazionale delle Ricerche, 40129 Bologna, Italy;* orcid.org/0000-0001-7244-4389; Email: marco.brucale@cnr.it

Authors

Lucrezia Caselli − *Consorzio Interuniversitario per lo Sviluppo dei Sistemi a Grande Interfase, 50019 Firenze, Italy; Dipartimento di Chimica "Ugo Schiff", Università degli Studi di Firenze, 50019 Firenze, Italy*

Matteo Baldoni − *Istituto per lo Studio dei Materiali Nanostrutturati, Consiglio Nazionale delle Ricerche, 40129 Bologna, Italy*

Costanza Montis − *Consorzio Interuniversitario per lo Sviluppo dei Sistemi a Grande Interfase, 50019 Firenze, Italy; Dipartimento di Chimica "Ugo Schiff", Università degli Studi di Firenze, 50019 Firenze, Italy*

Francesco Mercuri − *Istituto per lo Studio dei Materiali Nanostrutturati, Consiglio Nazionale delle Ricerche, 40129 Bologna, Italy;* orcid.org/0000-0002-3369-4438

Debora Berti − *Consorzio Interuniversitario per lo Sviluppo dei Sistemi a Grande Interfase, 50019 Firenze, Italy; Dipartimento di Chimica "Ugo Schiff", Università degli Studi di Firenze, 50019 Firenze, Italy;* orcid.org/0000-0001-8967-560X

Complete contact information is available at: https://pubs.acs.org/10.1021/acs.langmuir.1c01660

Notes

The authors declare no competing financial interest.

■ ACKNOWLEDGMENTS

This research received funding from the Horizon 2020 Framework Programme under the grants FETOPEN-801367 "evFOUNDRY" and FETPROACT-EIC-05-2019 "Bio-Organic Wetsuits". We thank the SPM@ISMN research facility for supporting the AFM experiments.

■ REFERENCES

(1) Van Niel, G.; D'Angelo, G.; Raposo, G. Shedding Light on the Cell Biology of Extracellular Vesicles. *Nat. Rev. Mol. Cell Biol.* **2018**, *19*, 213−228.

(2) Dulińska, I.; Targosz, M.; Strojny, W.; Lekka, M.; Czuba, P.; Balwierz, W.; Szymoński, M. Stiffness of Normal and Pathological Erythrocytes Studied by Means of Atomic Force Microscopy. *J. Biochem. Biophys. Methods* **2006**, *66*, 1−11.

(3) Hosseini, S. M.; Feng, J. J. How Malaria Parasites Reduce the Deformability of Infected Red Blood Cells. *Biophys. J.* **2012**, *103*, 1−10.

(4) Vorselen, D.; van Dommelen, S. M.; Sorkin, R.; Piontek, M. C.; Schiller, J.; Döpp, S. T.; Kooijmans, S. A. A.; van Oirschot, B. A.; Versluijs, B. A.; Bierings, M. B.; van Wijk, R.; Schiffelers, R. M.; Wuite, G. J. L.; Roos, W. H. The Fluid Membrane Determines Mechanics of Erythrocyte Extracellular Vesicles and Is Softened in Hereditary Spherocytosis. *Nat. Commun.* **2018**, *9*, 4960.

(5) Whitehead, B.; Wu, L.; Hvam, M. L.; Aslan, H.; Dong, M.; Dyrskjøt, L.; Ostenfeld, M. S.; Moghimi, S. M.; Howard, K. A. Tumour Exosomes Display Differential Mechanical and Complement Activation Properties Dependent on Malignant State: Implications in Endothelial Leakiness. *J. Extracell. Vesicles* **2015**, *4*, 29685.

(6) Rand, R. P.; Burton, A. C. Mechanical Properties of the Red Cell Membrane: I. Membrane Stiffness and Intracellular Pressure. *Biophys. J.* **1964**, *4*, 115−135.

(7) Dimova, R.; Riske, K. A. Electrodeformation, Electroporation, and Electrofusion of Giant Unilamellar Vesicles. In *Handbook of Electroporation*; SpringerLink, 2017; Vol. *1*, pp 235−252.

(8) van Mameren, J.; Wuite, G. J. L.; Heller, I. Introduction to Optical Tweezers: Background, System Designs, and Commercial Solutions. *Methods Mol. Biol.* **2018**, *1665*, 3−23.

(9) Krieg, M.; Fläschner, G.; Alsteens, D.; Gaub, B. M.; Roos, W. H.; Wuite, G. J. L.; Gaub, H. E.; Gerber, C.; Dufrêne, Y. F.; Müller, D. J. Atomic Force Microscopy-Based Mechanobiology. *Nat. Rev. Phys.* **2019**, *1*, 41.

(10) Parisse, P.; Rago, I.; Ulloa Severino, L.; Perissinotto, F.; Ambrosetti, E.; Paoletti, P.; Ricci, M.; Beltrami, A. P.; Cesselli, D.; Casalis, L. Atomic Force Microscopy Analysis of Extracellular Vesicles. *Eur. Biophys. J.* **2017**, *46*, 813−820.

(11) Piontek, M. C.; Lira, R. B.; Roos, W. H. Active Probing of the Mechanical Properties of Biological and Synthetic Vesicles. *Biochim. Biophys. Acta, Gen. Subj.* **2021**, *1865*, 129486.

(12) Calò, A.; Reguera, D.; Oncins, G.; Persuy, M.-A.; Sanz, G.; Lobasso, S.; Corcelli, A.; Pajot-Augy, E.; Gomila, G. Force measurements on natural membrane nanovesicles reveal a composition-independent, high Young's modulus. *Nanoscale* **2014**, *6*, 2275−2285.

(13) Sorkin, R.; Huisjes, R.; Bošković, F.; Vorselen, D.; Pignatelli, S.; Ofir-Birin, Y.; Freitas Leal, J. K.; Schiller, J.; Mullick, D.; Roos, W. H.; Bosman, G.; Regev-Rudzki, N.; Schiffelers, R. M.; Wuite, G. J. L. Nanomechanics of Extracellular Vesicles Reveals Vesiculation Pathways. *Small* **2018**, *14*, 1801650.

(14) Et-Thakafy, O.; Delorme, N.; Gaillard, C.; Mériadec, C.; Artzner, F.; Lopez, C.; Guyomarc'h, F. Mechanical Properties of Membranes Composed of Gel-Phase or Fluid-Phase Phospholipids Probed on Liposomes by Atomic Force Spectroscopy. *Langmuir* **2017**, *33*, 5117−5126.

(15) Takechi-Haraya, Y.; Goda, Y.; Sakai-Kato, K. Atomic Force Microscopy Study on the Stiffness of Nanosized Liposomes Containing Charged Lipids. *Langmuir* **2018**, *34*, 7805−7812.

(16) Di Santo, R.; Romanò, S.; Mazzini, A.; Jovanović, S.; Nocca, G.; Campi, G.; Papi, M.; De Spirito, M.; Di Giacinto, F.; Ciasca, G. Recent Advances in the Label-Free Characterization of Exosomes for Cancer Liquid Biopsy: From Scattering and Spectroscopy to Nanoindentation and Nanodevices. *Nanomaterials* **2021**, *11*, 1476.

(17) Canham, P. B. The Minimum Energy of Bending as a Possible Explanation of the Biconcave Shape of the Human Red Blood Cell. *J. Theor. Biol.* **1970**, *26*, 61−81.

(18) Helfrich, W. Elastic Properties of Lipid Bilayers: Theory and Possible Experiments. *Z. Naturforsch., C: Biochem., Biophys., Biol., Virol.* **1973**, *28*, 693−703.

(19) Vorselen, D.; Mackintosh, F. C.; Roos, W. H.; Wuite, G. J. L. Competition between Bending and Internal Pressure Governs the Mechanics of Fluid Nanovesicles. *ACS Nano* **2017**, *11*, 2628−2636.

(20) Boal, D. *Mechanics of the Cell*, 2nd ed.; Cambridge University Press, 2012.

(21) Landau, L. D.; Lifshitz, E. M. *Theory of Elasticity*, 3rd ed.; Course of Theoretical Physics, 1986.

(22) Wan, F. Y. M.; Gregory, R. D.; Milac, T. I. A Thick Hollow Sphere Compressed by Equal and Opposite Concentrated Axial Loads: An Asymptotic Solution. *SIAM J. Appl. Math.* **1998**, *59*, 1080−1097.

(23) Reissner, E. Stresses and Small Displacements of Shallow Spherical Shells I. *J. Math. Phys.* **1946**, *25*, 80−85.

(24) Reissner, E. Stresses and Small Displacements of Shallow Spherical Shells. I. *J. Math. Phys.* **1946**, *25*, 80−85.

(25) Vorselen, D.; Piontek, M. C.; Roos, W. H.; Wuite, G. J. L. Mechanical Characterization of Liposomes and Extracellular Vesicles, a Protocol. *Front. Mol. Biosci.* **2020**, *7*, 139.

(26) Tang, X.; Shi, X.; Gan, Y.; Yi, X. Nanomechanical Characterization of Pressurized Elastic Fluid Nanovesicles Using Indentation Analysis. *Extreme Mech. Lett.* **2020**, *34*, 100613.

(27) Kalluri, R.; LeBleu, V. S. The Biology, Function, and Biomedical Applications of Exosomes. *Science* **2020**, *367*, No. eaau6977.

(28) Richter, R. P.; Bérat, R.; Brisson, A. R. Formation of Solid-Supported Lipid Bilayers: An Integrated View. *Langmuir* **2006**, *22*, 3497−3505.

(29) Hardy, G. J.; Nayak, R.; Zauscher, S. Model Cell Membranes: Techniques to Form Complex Biomimetic Supported Lipid Bilayers

via Vesicle Fusion. *Curr. Opin. Colloid Interface Sci.* **2013**, *18*, 448−458.
(30) Clifton, L. A.; Campbell, R. A.; Sebastiani, F.; Campos-Terán, J.; Gonzalez-Martinez, J. F.; Björklund, S.; Sotres, J.; Cárdenas, M. Design and Use of Model Membranes to Study Biomolecular Interactions Using Complementary Surface-Sensitive Techniques. *Adv. Colloid Interface Sci.* **2020**, *277*, 102118.
(31) Caselli, L.; Ridolfi, A.; Cardellini, J.; Sharpnack, L.; Paolini, L.; Brucale, M.; Valle, F.; Montis, C.; Bergese, P.; Berti, D. A Plasmon-Based Nanoruler to Probe the Mechanical Properties of Synthetic and Biogenic Nanosized Lipid Vesicles. *Nanoscale Horiz.* **2021**, *6*, 543−550.
(32) Kanan, S. M.; Tze, W. T. Y.; Tripp, C. P. Method to Double the Surface Concentration and Control the Orientation of Adsorbed (3-Aminopropyl)Dimethylethoxysilane on Silica Powders and Glass Slides. *Langmuir* **2002**, *18*, 6623−6627.
(33) Ridolfi, A.; Caselli, L.; Montis, C.; Mangiapia, G.; Berti, D.; Brucale, M.; Valle, F. Gold Nanoparticles Interacting with Synthetic Lipid Rafts: An AFM Investigation. *J. Microsc.* **2020**, *280*, 194−203.
(34) Hutter, J. L.; Bechhoefer, J. Calibration of Atomic-Force Microscope Tips. *Rev. Sci. Instrum.* **1993**, *64*, 1868−1873.
(35) Ridolfi, A.; Brucale, M.; Montis, C.; Caselli, L.; Paolini, L.; Borup, A.; Boysen, A. T.; Loria, F.; Van Herwijnen, M. J. C.; Kleinjan, M.; Nejsum, P.; Zarovni, N.; Wauben, M. H. M.; Berti, D.; Bergese, P.; Valle, F. AFM-Based High-Throughput Nanomechanical Screening of Single Extracellular Vesicles. *Anal. Chem.* **2020**, *92*, 10274−10282.
(36) Nečas, D.; Klapetek, P. Gwyddion: An Open-Source Software for SPM Data Analysis. *Cent. Eur. J. Phys.* **2012**, *10*, 181−188.
(37) Marrink, S. J.; Tieleman, D. P. Perspective on the Martini Model. *Chem. Soc. Rev.* **2013**, *42*, 6801−6822.
(38) Alessandri, R.; Grünewald, F.; Marrink, S. J. The Martini Model in Materials Science. *Adv. Mater.* **2021**, *33*, 2008635.
(39) Summerfield, A.; Baldoni, M.; Kondratuk, D. V.; Anderson, H. L.; Whitelam, S.; Garrahan, J. P.; Besley, E.; Beton, P. H. Ordering, Flexibility and Frustration in Arrays of Porphyrin Nanorings. *Nat. Commun.* **2019**, *10*, 2932.
(40) Plimpton, S. Fast Parallel Algorithms for Short-Range Molecular Dynamics. *J. Comput. Phys.* **1995**, *117*, 1−19.
(41) Fernandez-Puente, L.; Bivas, I.; Mitov, M. D.; Méléard, P. Temperature and Chain Length Effects on Bending Elasticity of Phosphatidylcholine Bilayers. *Epl* **1994**, *28*, 181−186.
(42) Marsh, D. Elastic Curvature Constants of Lipid Monolayers and Bilayers. *Chem. Phys. Lipids* **2006**, *144*, 146−159.
(43) Li, S.; Eghiaian, F.; Sieben, C.; Herrmann, A.; Schaap, I. A. T. Bending and Puncturing the Influenza Lipid Envelope. *Biophys. J.* **2011**, *100*, 637−645.
(44) Hertz, H. Ueber Die Berührung Fester Elastischer Körper. *J. Reine Angew. Math.* **1882**, *92*, 156−171.
(45) Dimitriadis, E. K.; Horkay, F.; Maresca, J.; Kachar, B.; Chadwick, R. S. Determination of Elastic Moduli of Thin Layers of Soft Material Using the Atomic Force Microscope. *Biophys. J.* **2002**, *82*, 2798−2810.
(46) Åkesson, A.; Lind, T.; Ehrlich, N.; Stamou, D.; Wacklin, H.; Cárdenas, M. Composition and Structure of Mixed Phospholipid Supported Bilayers Formed by POPC and DPPC. *Soft Matter* **2012**, *8*, 5658.
(47) Leonenko, Z. V.; Finot, E.; Ma, H.; Dahms, T. E. S.; Cramb, D. T. Investigation of Temperature-Induced Phase Transitions in DOPC and DPPC Phospholipid Bilayers Using Temperature-Controlled Scanning Force Microscopy. *Biophys. J.* **2004**, *86*, 3783.
(48) Bilotto, P.; Lengauer, M.; Andersson, J.; Ramach, U.; Mears, L. L. E.; Valtiner, M. Interaction Profiles and Stability of Rigid and Polymer-Tethered Lipid Bilayer Models at Highly Charged and Highly Adhesive Contacts. *Langmuir* **2019**, *35*, 15552−15563.
(49) Charitat, T.; Bellet-Amalric, E.; Fragneto, G.; Graner, F. Adsorbed and Free Lipid Bilayers at the Solid-Liquid Interface. *Eur. Phys. J. B* **1999**, *8*, 583.
(50) Berquand, A.; Lévy, D.; Gubellini, F.; Le Grimellec, C.; Milhiet, P.-E. Influence of Calcium on Direct Incorporation of Membrane Proteins into In-Plane Lipid Bilayer. *Ultramicroscopy* **2007**, *107*, 928−933.
(51) Tristram-Nagle, S.; Petrache, H. I.; Nagle, J. F. Structure and Interactions of Fully Hydrated Dioleoylphosphatidylcholine Bilayers. *Biophys. J.* **1998**, *75*, 917−925.
(52) Daillant, J.; Bellet-Amalric, E.; Braslau, A.; Charitat, T.; Fragneto, G.; Graner, F.; Mora, S.; Rieutord, F.; Stidder, B. Structure and Fluctuations of a Single Floating Lipid Bilayer. *Proc. Natl. Acad. Sci. U.S.A.* **2005**, *102*, 11639−11644.
(53) Liu, Y.; Nagle, J. F. Diffuse Scattering Provides Material Parameters and Electron Density Profiles of Biomembranes. *Phys. Rev. E: Stat., Nonlinear, Soft Matter Phys.* **2004**, *69*, 040901.
(54) Levine, Z. A.; Venable, R. M.; Watson, M. C.; Lerner, M. G.; Shea, J.-E.; Pastor, R. W.; Brown, F. L. H. Determination of Biomembrane Bending Moduli in Fully Atomistic Simulations. *J. Am. Chem. Soc.* **2014**, *136*, 13582−13585.
(55) Picas, L.; Rico, F.; Scheuring, S. Direct Measurement of the Mechanical Properties of Lipid Phases in Supported Bilayers. *Biophys. J.* **2012**, *102*, L01−L03.
(56) Dimova, R. Recent Developments in the Field of Bending Rigidity Measurements on Membranes. *Adv. Colloid Interface Sci.* **2014**, *208*, 225−234.
(57) Nagle, J. F. Experimentally Determined Tilt and Bending Moduli of Single-Component Lipid Bilayers. *Chem. Phys. Lipids* **2017**, *205*, 18−24.
(58) Henriksen, J.; Rowat, A. C.; Brief, E.; Hsueh, Y. W.; Thewalt, J. L.; Zuckermann, M. J.; Ipsen, J. H. Universal Behavior of Membranes with Sterols. *Biophys. J.* **2006**, *90*, 1639−1649.
(59) Yi, Z.; Nagao, M.; Bossev, D. P. Bending Elasticity of Saturated and Monounsaturated Phospholipid Membranes Studied by the Neutron Spin Echo Technique. *J. Phys.: Condens. Matter* **2009**, *21*, 155104.
(60) Delorme, N.; Fery, A. Direct Method to Study Membrane Rigidity of Small Vesicles Based on Atomic Force Microscope Force Spectroscopy. *Phys. Rev. E: Stat., Nonlinear, Soft Matter Phys.* **2006**, *74*, 030901.
(61) Hochmuth, F. M.; Shao, J. Y.; Dai, J.; Sheetz, M. P. Deformation and Flow of Membrane into Tethers Extracted from Neuronal Growth Cones. *Biophys. J.* **1996**, *70*, 358−369.
(62) Redondo-Morata, L.; Giannotti, M. I.; Sanz, F. Influence of Cholesterol on the Phase Transition of Lipid Bilayers: A Temperature-Controlled Force Spectroscopy Study. *Langmuir* **2012**, *28*, 12851−12860.
(63) Gumí-Audenis, B.; Sanz, F.; Giannotti, M. I. Impact of Galactosylceramides on the Nanomechanical Properties of Lipid Bilayer Models: An AFM-Force Spectroscopy Study. *Soft Matter* **2015**, *11*, 5447−5454.
(64) Saavedra, V. O.; Fernandes, T. F. D.; Milhiet, P.-E.; Costa, L. Compression, Rupture, and Puncture of Model Membranes at the Molecular Scale. *Langmuir* **2020**, *36*, 5709−5716.
(65) LeClaire, M.; Gimzewski, J.; Sharma, S. A Review of the Biomechanical Properties of Single Extracellular Vesicles. *Nano Sel.* **2021**, *2*, 1−15.
(66) Berry, J. D.; Mettu, S.; Dagastine, R. R. Precise Measurements of Capsule Mechanical Properties Using Indentation. *Soft Matter* **2017**, *13*, 1943−1947.
(67) Vella, D.; Ajdari, A.; Vaziri, A.; Boudaoud, A. The Indentation of Pressurized Elastic Shells: From Polymeric Capsules to Yeast Cells. *J. R. Soc. Interface* **2012**, *9*, 448−455.

https://doi.org/10.1021/acs.langmuir.1c01660
Langmuir 2021, 37, 12027−12037